



CONSIDERATIONS IN THE DESIGN OF ELECTRICAL SUBSTATIONS, INCLUDING THE EFFECT OF POTENTIAL GRADIENT ON SURROUNDING METALLIC STRUCTURES

CONSIDERACIONES EN EL DISEÑO DE SUBESTACIONES ELÉCTRICAS, INCLUYENDO EL EFECTO DEL GRADIENTE DE POTENCIAL EN LAS ESTRUCTURAS METÁLICAS CIRCUNDANTES

Wilo Chilibingua¹ , Pablo Robles^{2,*} 

Received: 23-05-2022, Received after review: 13-06-2022, Accepted: 22-06-2022, Published: 01-07-2022

Abstract

For designing and studying an electrical substation grounding system (GS), a simple remote substation is considered according to the safety procedures indicated in the IEEE 80 Standard. Buried metallic materials or nearby metallic structures permanently endanger human life when electrical faults occur. Scenarios related to the design of electrical substations that consider the transfer of electrical potentials that can occur between the GS and buried metallic materials in their vicinity are presented, the behavior of potential transfer is evaluated, values of transferred voltages are calculated, and the main variables that influence the transferred voltage levels are identified. The simulations are performed with the CYMGRD software specific for GS calculations. Its analysis generates real results in the potential transfer that must be considered by the GS design engineer, which enables to avoid designing isolated substations without taking into account existing elements that may affect the substation surroundings.

Keywords: Electrical substation, grounding systems, ground grid, potential transfer, step and touch voltage, buried metal structures

Resumen

Para el diseño y el estudio de un sistema de puesta a tierra de una subestación eléctrica (*Grounding Systems, GS*, en inglés), se considera una subestación remota simple según los procedimientos de seguridad indicados en la norma IEEE 80. Los materiales metálicos enterrados o las estructuras metálicas cercanas ponen en peligro permanente la vida humana cuando se producen fallas eléctricas. Se presentan escenarios relacionados con el diseño de subestaciones eléctricas que consideran la transferencia de potenciales eléctricos que pueden producirse entre la GS y los materiales metálicos enterrados en sus proximidades. Se evalúa el comportamiento de la transferencia de potencial, se calculan los valores de las tensiones transferidas y se identifican las principales variables que influyen en los niveles de tensión transferidos. Las simulaciones se realizan con el programa CYMGRD específico para el cálculo de GS. Su análisis genera resultados reales en la transferencia de potencial que deben ser considerados por el ingeniero de diseño de GS, lo que permite evitar el diseño de subestaciones aisladas sin tener en cuenta los elementos existentes que pueden afectar al entorno de la subestación.

Palabras clave: subestación eléctrica, sistemas de puesta a tierra, red de tierra, transferencia de potencial, tensión de paso y de contacto, estructuras metálicas enterradas

¹Master of Electricity Program, Universidad Politécnica Salesiana, Quito, Ecuador.

^{2,*}Research Group on Smart Grids GIREI, IUS-RECI Electricity Grids and Smart Cities, Universidad Politécnica Salesiana, Cuenca, Ecuador. Corresponding author ✉: pablo121075@icloud.com

Suggested citation: Chilibingua, W. and Robles, P. "Considerations in the design of electrical substations, including the effect of potential gradient on surrounding metallic structures". *Ingenius, Revista de Ciencia y Tecnología*. N.º 28, (july-december). pp. 9-24. 2022. DOI: <https://doi.org/10.17163/ings.n28.2022.01>.

1. Introduction

The GS is an essential factor in human safety and maintenance of electrical inputs that make up a substation, considering its cost and durability [1]. In GS, ground fault currents must safely dissipate to return the ground to their sources; so that the protection devices can quickly disconnect the supply and eliminate the fault. However, fault currents flowing through the ground grid also flow through other buried metallic objects, including grounding systems connected to other facilities not affected by the faults [2], [3], [4], [5].

Although the GS may be physically isolated from each other, they are electrically linked through unwanted coupling, transferring dangerous electrical potentials from the meshes with fault currents to the non-energized passive meshes of other GS with a risk of electrocution for the personnel present. In those areas [6], [7], [8], [9]. Poor grounding in the oil and gas industry contributes to unnecessary downtime, but lack of good grounding is also dangerous and increases the risk of equipment failure leading to instrumentation errors, problems harmonic distortion, and power factor problems [10], [11,12].

Oil and gas pipelines are large and sophisticated structures protecting against electrical discharge, especially corrosion. For the design of the GS, cathodic protection [CP] must be included, in addition to the electrical effects that can occur when these two systems are together GS, and CP [13], [14], [15], [16], [17].

This article aims to present case studies on the problems introduced by the presence of metallic structures and adjoining protection systems, among others, in the transfer of potential gradients [GPG] in passive GS.

The design procedures described in the standards related to GS of electrical substations in urban areas and oil stations allow the calculation of safe levels of step and touch voltages within the substation area, but adjacent GPG is not taken into account [18], [19], [20], [21], [22], [23], [24].

The type of material used can be a decisive factor in human electrocution. Inside the substations, the touch voltage [MTV] and step voltage [MSV] are less dangerous due to the high resistivity surface layer [25]. However, this layer does not extend outside the substations, where the transferred touch and step voltages can be harmful and much more if there are adjoining buried metallic structures not connected to the GS [26], [27], [28]; [29].

1.1. Related Works

The potential gradient generated [30], [31] in oil refining complexes in the event of a failure in an electrical substation causes its transfer to the process areas, causing damage to the instrumentation system, [32,33].

Metallic parts such as water and gas pipes, rails, and building foundations can modify the distribution of electrical potential in the area, depending on the structural topology, which triggers the effect of the GPG, [8].

The GS must consider the conductors directly involved in the protected installation, and any other, connected or not, can interact with the whole GS (Figure 1).

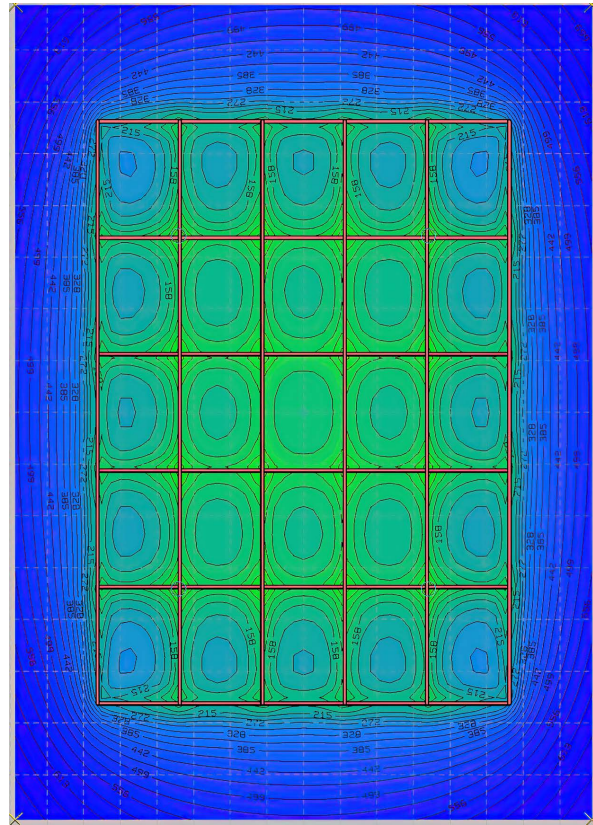


Figure 1. Equipotential contour of a mesh of one GS

The pipelines carrying harmful products are protected against corrosion, usually by layers of coating materials integrated with active cathodic protection systems [34,35]. The current flow, typically adopted for large or long structures, force the pipe to behave as a cathode, thus providing corrosion protection of its exposed parts when the coating fails. However, buried lines with cathodic protection, close to the grounding networks of electrical substations, allow the possibility of bonding and reduce the risk of metal-to-metal contact voltages. This bonding connection, necessary for the safety of operating personnel, can compromise the CP's effectiveness. To avoid corrosion of the CP and bonding with the mesh, mineral salts, which ionize, forming a solid electrolyte with a pH varying from 8 to 10, must be considered.

In electrical substations in urban areas, metal parts that can modify potential electrical distribution are

2. Materials and methods

2.1. Problem Formulation

Figure 2 presents a flow chart of the electrical substation design methodology, including the effect of the potential gradient on the surrounding metallic structures, where the designer's expertise allows obtaining results according to the threshold contact voltages and the threshold step voltage.

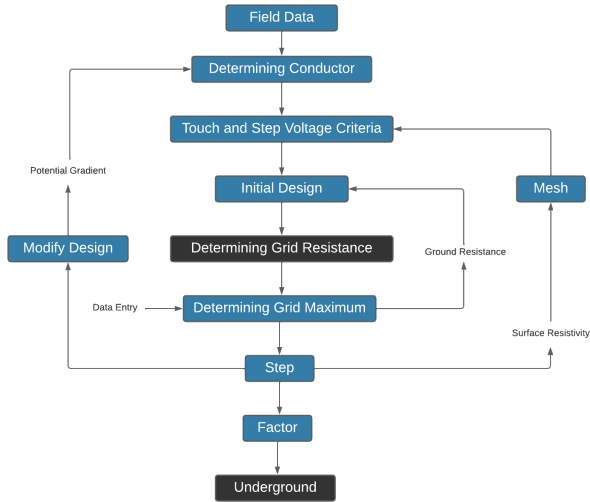


Figure 2. Methodology used for the design

Case studies are presented, which will allow analyzing the transfer of potential. The simulation of the scenarios is carried out with specialized CYMGRD software using the finite element method (FEM) developed by EATON; it allows the interpretation of soil resistivity measurements, elevation of earth potential, and evaluation of dangerous points in any area of additional interest, generates a visual representation of the results of the analysis on the potential of the mesh. The proposed scenarios are according to the type of surface layer used and the potential transfer analysis; the input data presented correspond to the following:

Table 3. General Notation & Descriptions

| Nomenclature | Description |
|---------------------------------------|---------------------------|
| <i>Uniform</i> | Terran Model |
| ρ 50 Ω - m | Upper layer resistivity |
| 40°C | Ambient temperature |
| 0.15 μ m | Surface layer thickness |
| ρ_s -200 Ω -m - concrete | Surface layer resistivity |
| ρ_s - 5000 Ω -m - gravel | Surface layer resistivity |
| ρ_s -10000 Ω -m - asphalt | Surface layer resistivity |
| 0.1sec | Fault duration time |
| 10kA | Fault current |
| 50kg | Human body mass |
| Sf100V | Current division factor |
| Cp100V | Growth factor |
| 1m | Mesh depth |
| Cu4 - 0AWG | Conductor Cu |

The present study focuses on the variation of the surface layer, the physical location of the mesh, and the different locations of the surrounding metallic structures.

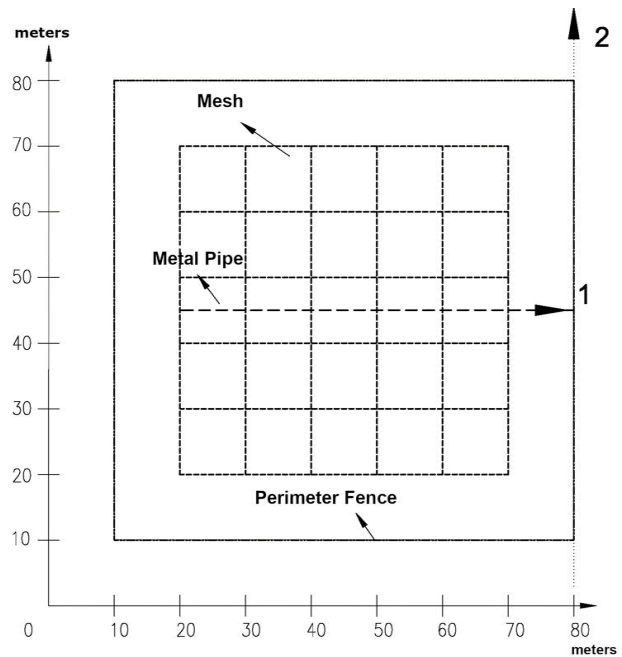


Figure 3. Top view of GS case study 1

In the case of asymmetric grids, the analysis study is similar; taking the stratigraphy of the terrain, the exposed potential gradients transfer study metric is applied for any grid configuration.

Parameter values of the GS are taken based on the mesh indicated in figure 3 so that the importance of step and touch voltage does not exceed the maximum allowed values; the use of copper rods or electrodes is not considered for these simulations.

For the design and simulation of the scenarios, the bodyweight of a 50kg person is taken.

Assuming the most sensitive case that can occur, the optimal mesh conductor for this configuration is a copper conductor of 20.3776 mm², equivalent to 2/0 AWG for the simulations of the scenarios, a 4/0 AWG copper conductor is taken up, where the IEEE 80 standard suggests considering the effects of corrosion present by the PH of the soil stratigraphy, [22].

2.1.1. Case Study 1

Figure 3 shows a substation grounding mesh; its dimensions correspond to 50×50 meters with 10-meter grids; the perimeter conductor GS at 1 m depth in uniform soil with a straight metallic cylindrical tube at 2 m depth.

It is analyzed such as a) effects are produced by the transfer of potentials in the mesh when having the presence of an underground metal perimeter fence, and b) the effects are due to potential transfers caused

by the presence of a metallic pipe buried under the GS.

For the analysis, different configurations of the GS and the underground pipeline.

Potentials are analyzed in an asymmetric mesh; a case presented depending on the topology and the facilities offered by its on-site construction.

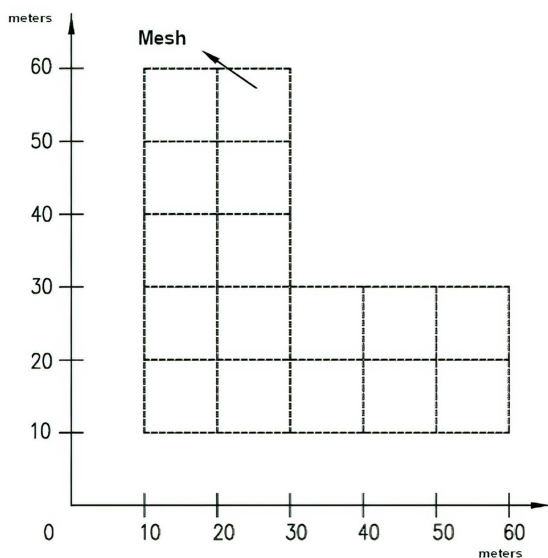


Figure 4. Top view of asymmetrical L-type mesh

2.1.2. Case Study 2

In Figure 5, rails located at a distance "d" from the mesh are added; for study case 2, the transfer of potential is reflected in changes of touch, step, GPG, and R_g voltages that occur in the directions will be analyzed indicated.

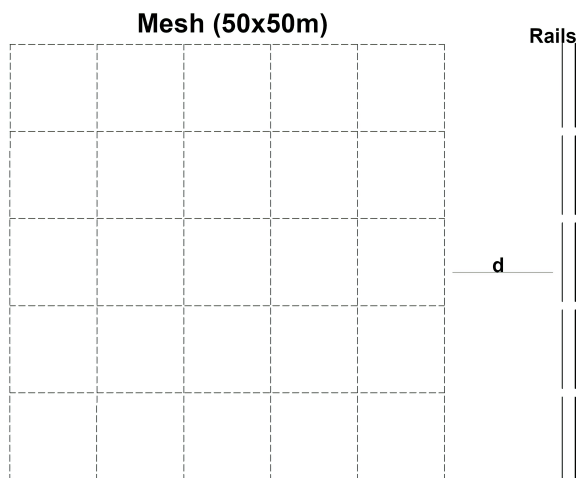


Figure 5. Top view Mesh - Rails

2.1.3. Case Study 3

The mutual interference of nearby ground grids is analyzed to assess the potentially dangerous circumstances in sites protected by the primary grid, including proximity to an adjoining one that dissipates the ground fault current in the surrounding ground, mainly in urban areas, a) mesh 1 Main and Mesh 2 Offline, b) mesh one primary and mesh two connected, c) mesh one primary and Mesh 2 are connected to other GS.

Two meshes of the grounding system are considered, with similar topology and technical parameters. Adjacent edges of the meshes are spaced a distance d meters apart.

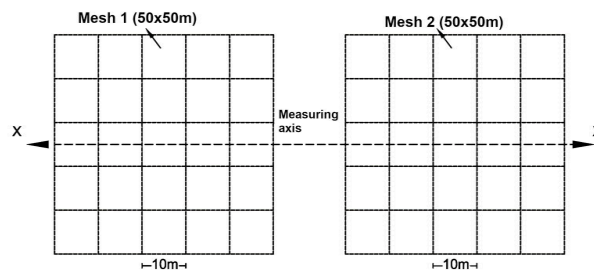


Figure 6. Nearby grounding grids

2.2. Interferences between GS and cathodic protection.

The standards and recommended practices for the design of cathodic protection systems establish the need to interconnect metallic structures with each other. However, this equipotential bonding can compromise cathodic protection and safety effectiveness. GS traditionally built with copper electrodes, due to their stability characteristics over time, present problems concerning cathodic protection: a copper ground mesh connected to the structure under cathodic protection can drain a considerable amount of the protection current. It may be impossible to polarize the steel structure correctly in specific scenarios. If the cathodic protection is no longer adequate, corrosion is at risk due to a galvanic coupling between copper and steel.

2.3. Impact of ground faults on pipelines and possible solutions.

Destructive electrical arcs can be prevented by bonding the GS to the pipe. However, such a connection would cause the cathodic protection system to drain; this is solved by inserting an ISP or a polarization cell in said connection. The fault current impressed on the pipe must be safely dissipated to earth employing uncoupled intentional sacrificial anodes, e.g., magnesium or zinc materials, connected and installed along the pipe with a low resistivity. These sacrificial anodes would also facilitate the dissipation to the ground of currents

conducted to the pipeline from locations remote from the substation area.

Instead of bonding conductors, installing decoupling devices, such as insulator surge protectors between grounding electrodes and pipelines, is the best compromise to safeguard safety and functionality during ground faults. Decouplers minimize the impact of ground faults on channels while preserving the effectiveness of the cathodic protection.

Human safety depends on the energy absorbed before the fault is cleared and the system is deactivated; it is suggested to establish step voltage and touch voltage limits which are called thresholds, depending on the material used as the surface layer and its reduction factor, Dalziel and Lee set constants related to the electrical discharge energy tolerated.

3. Results and discussion

3.1. Analysis of Results

3.1.1. Effects of perimeter mesh earth conductor

The underground metallic pipe is not considered; the contour and profile graphs of the potential gradient of the cases are made, considering the finished floor as the asphalt $\rho_s = 10000\Omega - m$.

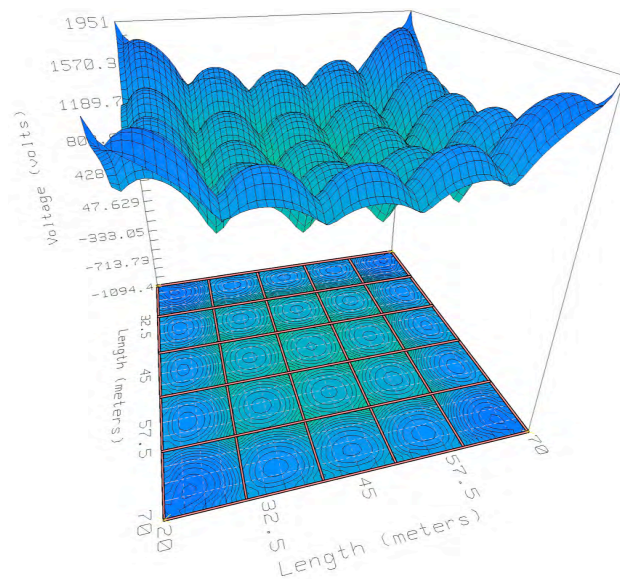


Figure 7. Touch voltage, insulated mesh- ρ_s asphalt

The underground metallic pipe is not considered; the contour and profile graphs of the potential gradient of the cases are made, considering the finished floor as the asphalt (Figure 7 and 8). Ground mesh and perimeter fence without connection see (Figure 9 and 10).

A summary of the simulations with the conditions set out for study case 1, with surface layers of concrete, gravel, and asphalt is presented.

At $\rho_s = 200\Omega - m$ concrete, the touch and step threshold voltages correspond to 457.82 V and 730.83 V.

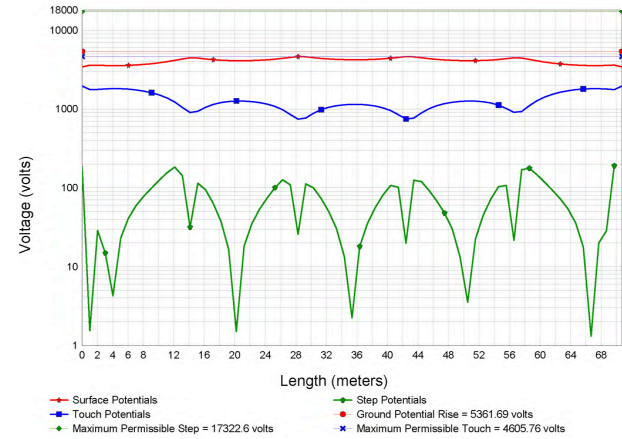


Figure 8. Insulated mesh potential profile - ρ_s asphalt

Table 4. Mesh and perimeter fence without connection

| Cases | $\rho_s = 200\Omega - m$ concrete | | |
|---------------------------------------|-----------------------------------|-------------|---------|
| | MTV_{max} | MSV_{max} | GPG |
| Insulated mesh IM | 1951.02 | 190.26 | 5361.69 |
| Profile address 1 PA1 | 1455.92 | 119.73 | 5361.69 |
| Profile address 2 PA2 | 3599.08 | 35.53 | 5361.69 |
| Mesh-Net without connection MNWC | 1015.99 | 89.43 | 3932.32 |
| Profile address 1 no connection PA1NC | 873.31 | 57.63 | 3932.32 |
| Profile address 2 no connection PA2NC | 1392.32 | 92.61 | 3932.32 |

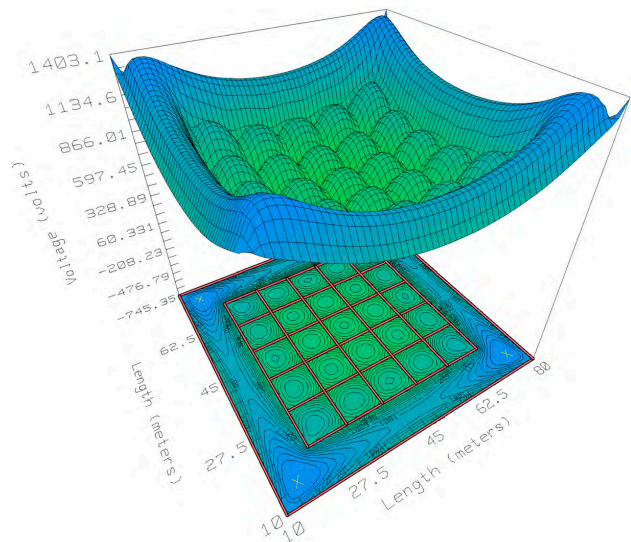


Figure 9. Touch voltage, mesh and fence without asphalt- ρ_s connection

Changing for a finished gravel floor, $\rho_s = 5000\Omega - m$, the threshold voltages of touch and step vary to

2489.47 V and 8857.39 V, with the change to asphalt $\rho_s = 10000\Omega - m$, touch and step voltages thresholds are 4605.76 V and 17322.6 V. The material used as surface layer allows to have a mesh resistance R_g at 0.476 Ω and for an isolated mesh with near no connection at a value of 0.35 Ω . The maximum touch voltages [MTV], maximum step voltage [MSV], and GPG see the Table 4.

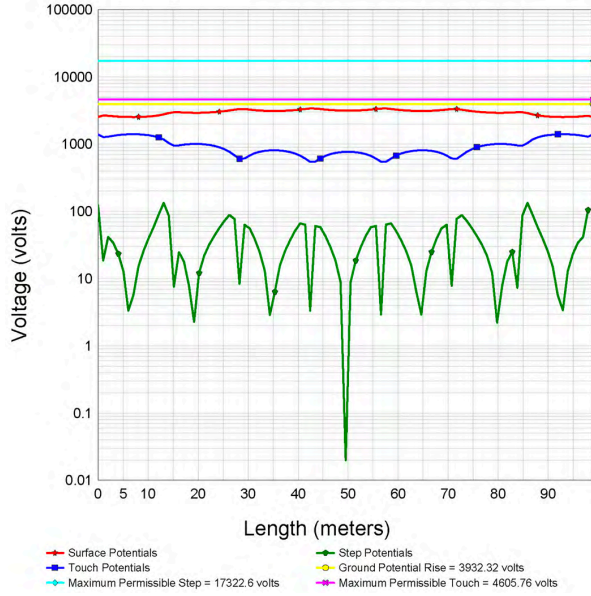


Figure 10. Potential mesh and fence profile without asphalt- ρ_s connection

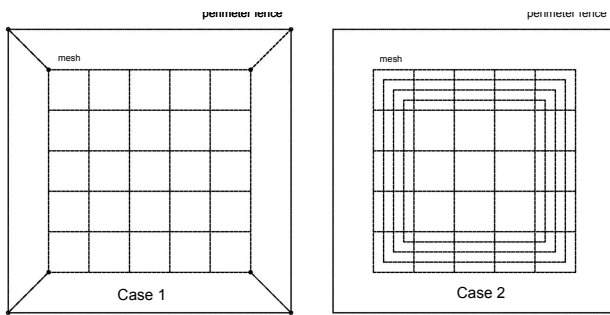


Figure 11. Modified mesh and mesh connected to fence

According to the simulations carried out with different values of the surface layer, the threshold touch voltages [TTV] and threshold step voltage [TSV] are directly related to the surface layer’s resistivity. The change of material in the surface layer to gravel or asphalt allows the touch voltages, step voltage, GS, and R_g to vary in favor of the safety of the human being when the perimeter fence is implanted. The surface layer of concrete allows the MTV to exceed the values of TTV and TSV, which suggests improving the architecture of the mesh. Based on the mesh and perimeter fence indicated in figure 3, the modifications

made to the architecture of the mesh to reduce the MTV and MSV when there is a surface $\rho_s = 200 \Omega\text{-m}$, suggest a) attach the mesh to the perimeter fence, b) modify the mesh, increasing more loops on the outer parts. See figure 11. In case 1, with the architecture change, the TTV and TSV correspond to 457.82V and 730.83V, the $R_g = 0.34\Omega$ does not vary, and the MTV and MSV, as well as the GS, are shown in Table 5.

Table 5. Mesh and Perimeter Mint

| $\rho_s = 200\Omega - m$ [concrete] | | | |
|---|--------|--------|---------|
| Cases | MTV | MSV | GPG |
| Mesh and fence connected [MFC] | 936,7 | 83,54 | 3858,7 |
| Modified mesh without connection [MMWC] | 851,86 | 150,73 | 3836,26 |

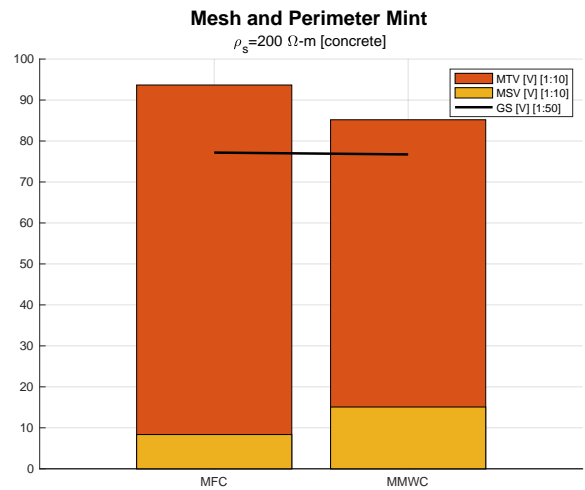


Figure 12. Metric with mesh architecture change

3.1.2. Influence of the perimeter mesh

The results allow us to observe the effects of the perimeter fence on the MTV, MSV, GPG, and R_g : If the earth conductor of the perimeter fence encloses the substation mesh, its effects on the MTV of the mesh decrease up to 48%, and the GS and R_g decrease by 27%. The most typical configurations used to decrease the touch voltage are observed in figure 11; in table 5, the MTV and MSV decrease in case 1. In case 2, with the modified mesh, the MTV decreases, and MSV increases concerning the values indicated in table 3 when there is a mesh and fence without a connection. If the GS increases, the R_g increases; this is logical since the GS is proportional to R_g , according to its formula, $GPG = I_g \cdot R_g$. When the GS increases, the peak touch voltage decreases. In case 1, mesh and fence connected, the maximum voltage value decreases by 8%, especially where the mesh and rail are not connected. In case 2, modified mesh, the maximum touch voltage decreases by 16% for the case in which the mesh is present and the fence is offline.

3.1.3. The buried metal pipe effects

For the analysis of the effects of the pipe on the ground grid, the fence indicated in figure 2 is not taken into account; the touch, step, and GS voltage simulations are carried out on the grid and direction 1. Metal pipe of a fixed diameter, buried at different depths. See Table 5. A metal pipe is buried at a fixed depth and variable diameters. See Table 6. An example of item a is simulated, with a surface layer of asphalt for the case of a 400 mm Ø pipe case and a depth of 2m, Table 6.

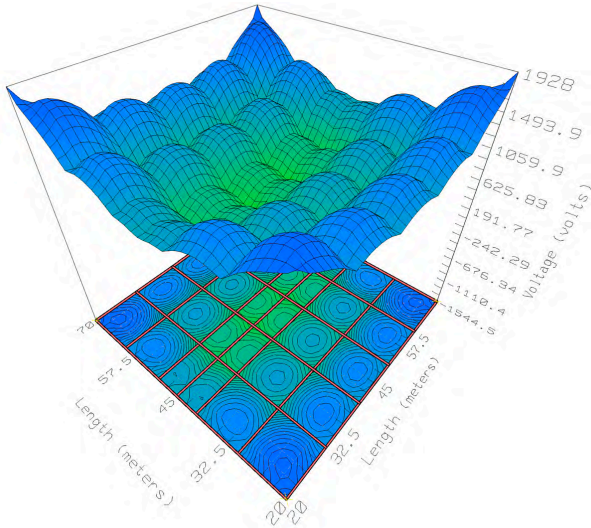


Figure 13. Touch voltage, mesh and asphalt- ρ_s pipe

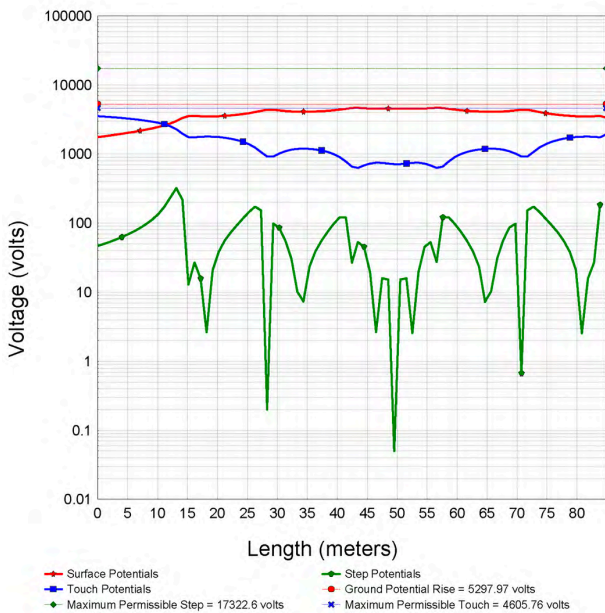


Figure 14. Potential direction profile 1 - mesh and pipe - ρ_s asphalt

A summary of the simulations carried out with pipes of different diameters, depths, and surface

layers of concrete, gravel, and asphalt are present. $\rho_s = 200\Omega - m$ [concrete], constant diameter pipe, and underground metallic line at depths of 2, 3, 4, and 5 m, TTV, and TSV correspond to 457.82 V and 730.83 V when changing the scenario For the surface layer of gravel [$\rho_s = 5000\Omega - m$], the TTV and TSV vary between 2489.47 V and 8857.39 V, for the case of asphalt as a surface layer being its $\rho_s = 10000\Omega - m$, the TTV. TSV equal 4605.76 V and 17322.6 V, R_g is set to 0.47Ω . The maximum touch, step, and PG voltages present a variation presented in Table.

Table 6. Constant pipe diameter and variable depth

Mesh and underground piping (diameter 400 mm)

$\rho_s = 200\Omega - m$ [concrete]

$\rho_s = 5000\Omega - m$ [gravel]

$\rho_s = 10000\Omega - m$ [asphalt]

| | | | |
|---------------------------|---------|--------|---------|
| Mesh - Pipe 2m [MP2] | 1924.62 | 186 | 5288.62 |
| Profile Address 11 [PD11] | 1053.52 | 113.23 | 5288.62 |
| Mesh - Pipe 3m [MP3] | 1911.75 | 184.93 | 5263.10 |
| Profile Address 12 [PD12] | 1090.21 | 112.56 | 5263.10 |
| Mesh - Pipe 4m [MP4] | 1897.24 | 183.78 | 5235.02 |
| Profile Address 13 [PD13] | 1114.58 | 111.75 | 5235.02 |
| Mesh - Pipe 5m [MP5] | 1881.5 | 182.56 | 5204.92 |
| Profile Address 14 [PD14] | 1131.21 | 110.75 | 5204.92 |

$\rho_s = 200\Omega - m$ [concrete], pipe diameter variation at 0.8, 0.6, 0.4, 0.2m at constant depth, TTV and TSV at 457.82V and 730.83V, yes gravel with $\rho_s = 5000\Omega - m$ is used as a surface layer, TTV and TSV indicate values in 2489.47 V and 8857.39V. For the scenario of using asphalt as the surface layer, knowing that its $\rho_s = 10000\Omega - m$, the result corresponds to 4505.76 V and 17322.6 V, indicating that $R_g = 0.47\Omega$. The MTV, MSV, and PG present a variation presented in Table 7.

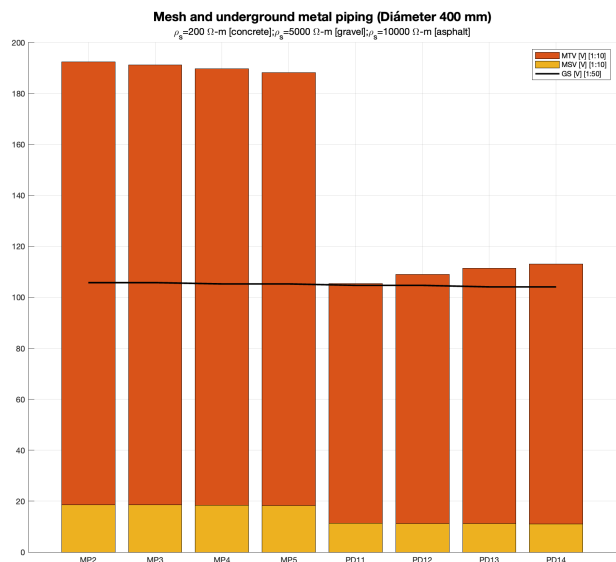


Figure 15. Metric mesh and underground metallic pipe

Table 7. Variable diameter and constant depth pipe - ρ concrete

Mesh and underground metal piping (2m)
 $\rho_s = 200\Omega - m$ [concrete]
 $\rho_s = 5000\Omega - m$ [gravel]
 $\rho_s = 10000\Omega - m$ [asphalt]

| Cases | MTV | MSV | GPG |
|--|---------|--------|------------|
| Mesh - Pipe \varnothing 0.8m [MP0.8] | 1920.08 | 185.26 | 5276.08.62 |
| Profile Address 11 [PD11] | 998.72 | 112.12 | 5276.08 |
| Mesh - Pipe \varnothing 0.6m [MP0.6] | 1922.13 | 185.59 | 5261.76 |
| Profile Address 12 [PD12] | 1018.71 | 112.62 | 5261.76 |
| Mesh - Pipe \varnothing 0.4m [MP0.4] | 1924.62 | 186 | 5288.62 |
| Profile Address 13 [PD13] | 1053.62 | 113.23 | 5288.62 |
| Mesh - Pipe \varnothing 0.2m [MP0.2] | 1927.98 | 186.54 | 5297.97 |
| Profile Address 14 [PD14] | 1104.79 | 114.06 | 5297.97 |

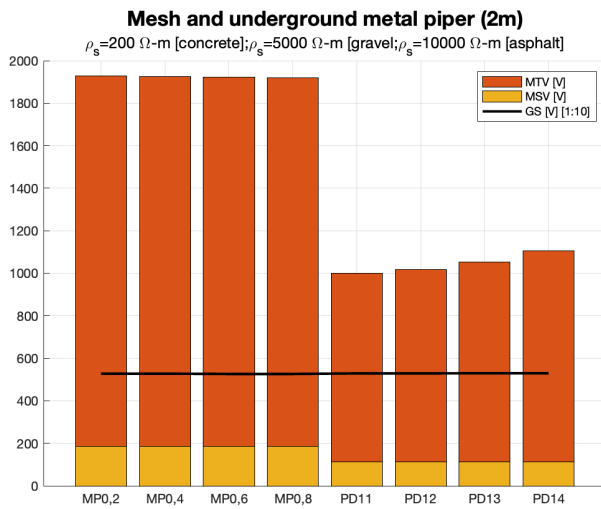


Figure 16. Display of values Table 8

In the presence of an underground metal pipe that crosses under the mesh, with a constant diameter and variable depth, the MTV and MSV decrease the deeper it is, while the R_g and GS do so on a smaller scale. If its diameter is variable and its depth constant, the MTV and MSV increase when the pipe diameter decreases, and the R_g and GS increase to a lesser extent. In figure 3, different scenarios are proposed, keeping constant the parameters of the mesh, diameter, and variable depth, the objective of these configurations allows to determine which strategy is more favorable for the decrease of TTV and TSV that can be generated on the surface area of the pipeline when a fault occurs in the electrical system.

3.1.4. Analysis of results of underground metallic pipelines

The voltages MTV [457.82 V] and MSV [730.83 V] of case 1 indicated in table 1 are taken as reference, where it is recommended to install more ground mesh conductors parallel to the underground pipe that passes below; this helps to decrease the TTV and TSV in the

mesh, due to the increase in electromagnetic fields. Another way to reduce TTV and TSV is to make the pipe cross diagonally as much as possible. An exhaustive analysis suggests underground pipes leave an electrical substation area because voltage-transfer generates GPG and TTV values higher than those admissible for its configuration. In these cases, installing copper weld rods attached to the beginning and end of the pipe is recommended. According to the studies carried out on the metallic pipe, it is possible to observe that this affects the potential of the mesh.

When inside the grid area, the buried metal pipe decreases the TTV and TSV; in real situations, this does not happen because the pipes always enter and leave the grid area. When a metal pipe leaves or is outside the mesh area, it causes elevation of TTV and GPG in regions outside the mesh; this is logical since by increasing the length of the pipe, the increase in potential will approach the rise in network potential. When a fault occurs in the electrical system, a current is generated in the pipe; this increases when the pipe is further away. The scenarios presented with underground metallic pipes clearly show the danger of transferred potentials. For GS designs in electrical substations, corrective measures must be taken when metallic structures are nearby; the designer must know their influence with acceptable precision; otherwise, they may apply erroneous or unjustified measures.

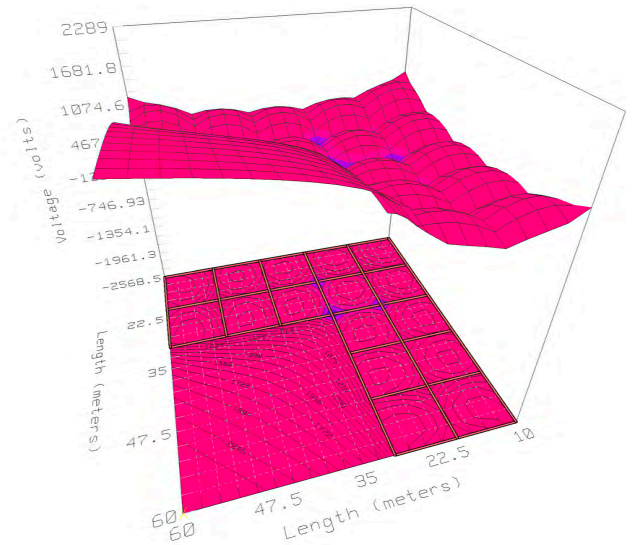


Figure 17. Asymmetrical mesh touch voltage - ρ_s concrete

According to sound engineering practices, corrective procedures are in place to minimize the transfer of potential when metallic structures are buried. Joining the metallic structure to the main mesh, however, the consequences of the said procedure is carefully verified due to the possible transfer of the increase in the potential of the networks [reverse situation]. Provide denser meshes for the grid over the buried pipe. These

meshes can, in some cases, act as a protective mesh by reducing the magnitude of the touch voltage. Install insulating flanges on underground metal piping at suitable locations. The optimal solution in the corrective methods to be used will depend on several factors, such as the properties of the soil, the location of the metallic structure, and the fault current, among others.

3.1.5. Mesh Type L

An GS study of an asymmetric mesh is presented, see figure 4, for this case, a surface layer of resistivity $\rho_s = 200\Omega - m$ [concrete] is considered, obtaining the values shown in Table 8.

Table 8. Asymmetric mesh type L

| Cases | Asymmetric mesh type L $\rho_s = 200\Omega - m$ [concrete] | | | | | GPG [V] |
|----------------|---|---------|--------|--------|-------------|---------|
| | MTV | MSV | TTV | TSV | $R_g\Omega$ | |
| Insulated mesh | 457,82 | 2288,99 | 730,83 | 132,11 | 0,56 | 3168 |

In the exposed case, it is observed that with the surface layer of concrete, the MTV exceeds the MSV; in figure 16, the procedures to improve the TTV are the same as those exposed in symmetric or asymmetric meshes.

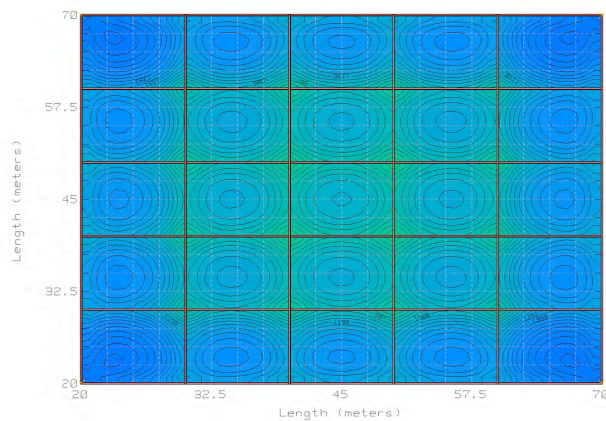


Figure 18. Mesh potential contour - without rails

3.1.6. Analysis of results Scenario 2

A mesh and nearby rails are considered, the configuration of the mesh indicated in figure 3 is used, the study is made based on what is shown in figure 5, and a surface layer of asphalt is considered.

3.1.7. Case 2.1 Ground grid without considering nearby rails

An analysis of the potential contour of the ground grid is made without considering the rails; figure 18 shows the potential distribution on the ground surface when a fault condition occurs.

3.1.8. Case 2.2 Ground Grid considers rails without connection to the grid

It is proposed to analyze the potential contour of the ground grid considering the rails at a distance $[d=30m]$ without connection; this is a common situation in electrical substations and power plants, the simulation of the rails is done through steel conductors 90 mm diameter aluminum-clad separated at a distance of 1.5 m and a length of 50 m. Figure 19.

3.1.9. Case 2.3 Earth grid considering the rails connected to the grid

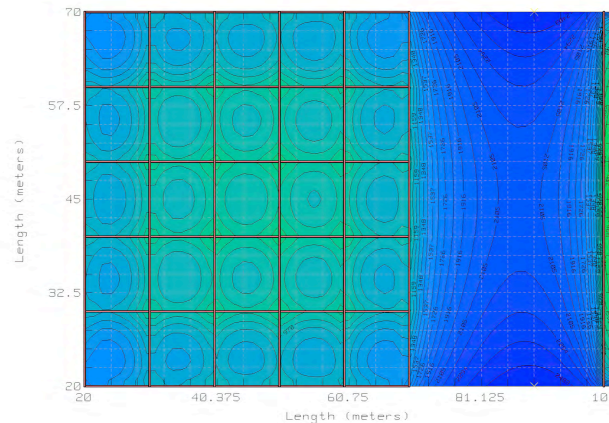


Figure 19. Mesh potential contour - with rails

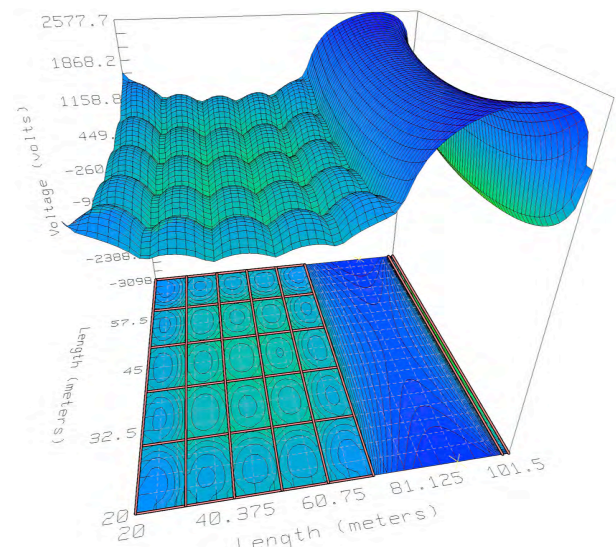


Figure 20. Touch voltage mesh and rails without connection

The potential contour of the ground grid, considering the rails connected to the ground grid employing 4/0 AWG copper cables at 5 points uniformly distributed on the rails, is presented as a case study. See figure 20. Figures 17, 18, and 19 show the change in potential curves when the rails are installed; the most

important differences can be seen in the distribution of potentials in the surroundings since high GS are generated to be considered. Figures 19 and 20 show that the TTV values increase in the area between the rails and the mesh when they are not connected; they are joined with the mesh to reduce these potentials. Figures 21 and 22.

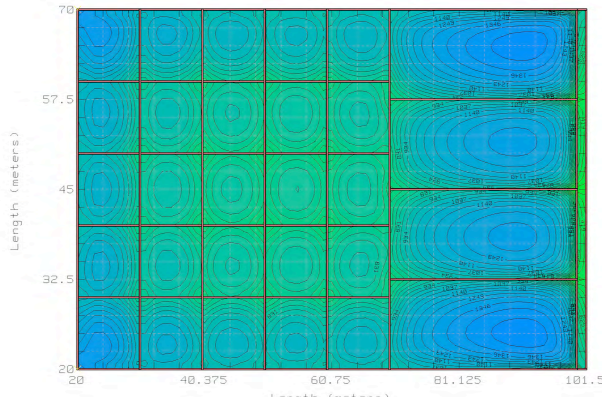


Figure 21. Mesh potential contour with rail connection

Table 9. Variable diameter and constant depth pipe - ρ concrete

| Mesh and Rails (Rail Diameter 90mm, Depth 10mm) | | | | |
|---|---|---------|--------|---------|
| $\rho_s = 10000\Omega - m$ [asphalt] | | | | |
| Item | Cases | MTV | MSV | GPG |
| 1 | Insulated Mesh [IM] | 1951.02 | 190.26 | 5361.69 |
| 2 | Potential Rails [PR1] | 3984.13 | 9.57 | 5361.69 |
| 3 | Mesh and Rails without Connection 1 [MRWC1] | 1651.47 | 152.99 | 4606.32 |
| 4 | Rail Potentials [PR2] | 1739.38 | 576.69 | 4606.32 |
| 5 | Mesh - Pipe \varnothing 0,4m [MP0,4] | 1924.62 | 186 | 5288.62 |
| 6 | Potential Rails [PR3] | 717.73 | 227.69 | 4201.47 |
| 7 | Mesh and Rails without Connection 2 [MRWC2] | 1671.74 | 155.12 | 4657.38 |
| 8 | Isolated Potential Rails [PRA] | 1606.9 | 756.61 | 4657.38 |

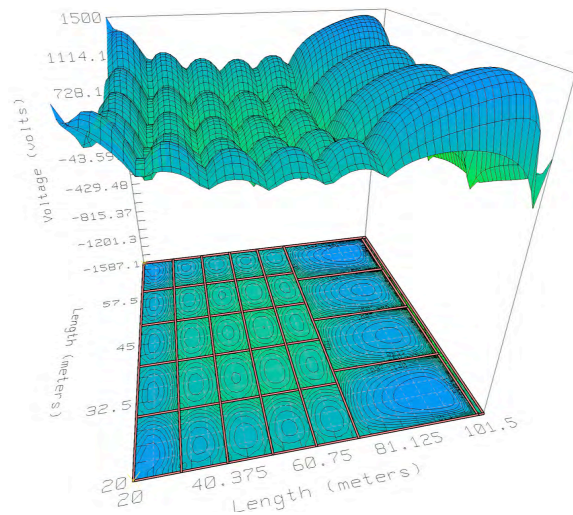


Figure 22. Voltage of touch screen and connected rails

If the rails are not connected to the mesh, the TTV and TSV values are high, see Table 9, item 2, if they

are connected to the mesh, they decrease, and the GP and R_g values. Another way to reduce the potentials in the rails when they are not connected to the mesh is to insulate the union joints, see Table 9, item 8; in the same way, the rails can be grounded using metal rods or copper-weld.

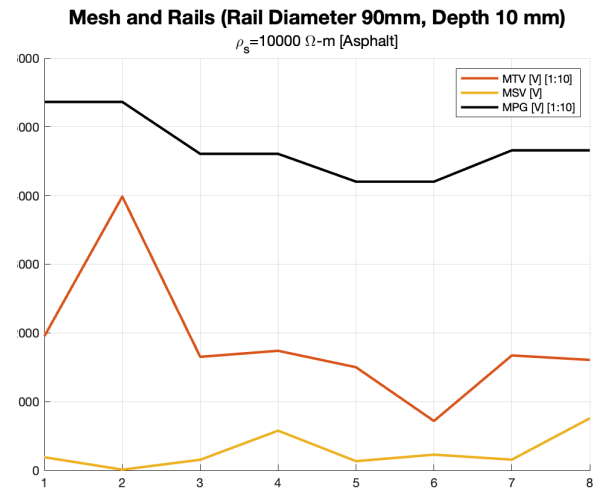


Figure 23. Display of values table 6

3.1.10. Analysis of Results Scenario 3

Mesh 1 and mesh two are considered; Figure 6, the mesh configuration indicated in figure 3 is used with a surface layer of gravel and a short-circuit current of 10 kA.

3.1.11. Mesh 1 and Mesh 2 No Connection

When an electrical fault occurs in mesh 1, it affects mesh two due to the difference between the potentials of the ground surface and the potential in mesh 2; the simulation for the two meshes is done by varying their distance, starting from 10 up to 120 meters; obtaining TTV= 2489.47 V and TSV=8857.39 V.

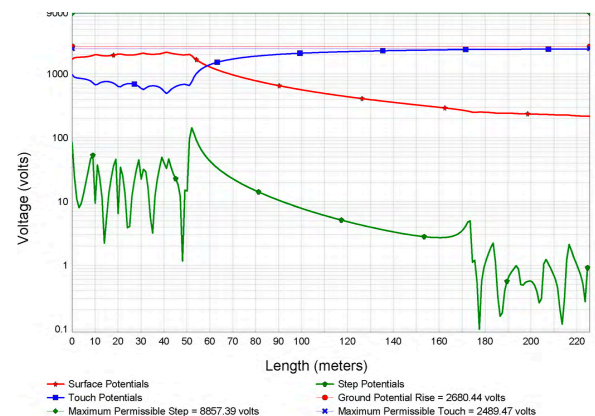


Figure 24. Touch and step voltage on the measuring axis of the meshes. Mesh 1 and Mesh 2 without connection

Table 10. Voltages touch step R_g GPG – Insulated mesh

| d(m) | Mesh 1 | | | | Mesh 2 | | | |
|------|-----------------|-------|-------------|---------|-----------------|-------|-------------|---------|
| | Maximum Voltage | | $R_g\Omega$ | GPG | Maximum Voltage | | $R_g\Omega$ | GPG |
| | Touch | Step | V | Touch | Step | V | V | |
| 10 | 980.754 | 96.58 | 0.468 | 2636.63 | 2054.55 | 22.64 | 0.468 | 734.951 |
| 20 | 978.146 | 95.8 | 0.473 | 2661.43 | 2165.5 | 14.71 | 0.473 | 607.649 |
| 30 | 976.994 | 95.49 | 0.474 | 2670.57 | 2234.7 | 10.86 | 0.474 | 522.136 |
| 40 | 976.354 | 95.33 | 0.475 | 2674.82 | 2284.7 | 8.44 | 0.475 | 409.968 |
| 50 | 976.009 | 95.26 | 0.476 | 2677.06 | 2323.38 | 6.77 | 0.476 | 409.968 |
| 60 | 975.806 | 95.21 | 0.476 | 2678.34 | 2354.56 | 5.56 | 0.476 | 370.686 |
| 70 | 975.693 | 95.18 | 0.476 | 2679.11 | 2380.38 | 5.64 | 0.476 | 382.68 |
| 80 | 975.629 | 95.17 | 0.476 | 2679.61 | 2420.21 | 3.93 | 0.476 | 311.425 |
| 90 | 975.588 | 95.16 | 0.476 | 2679.94 | 2420.96 | 3.41 | 0.476 | 288.475 |
| 100 | 975.554 | 95.14 | 0.476 | 2680.16 | 2437.25 | 3.99 | 0.476 | 268.717 |
| 110 | 975.543 | 95.14 | 0.476 | 2680.32 | 2451.58 | 2.65 | 0.476 | 251.521 |
| 120 | 975.528 | 95.14 | 0.476 | 2680.4 | 2464.27 | 2.36 | 0.476 | 236.414 |

The MTV generated by mesh 1 in mesh 2 grow as they move away, reaching their maximum value of 2464.27 V at a distance of 120m; otherwise, the MSV decreases as they move away. In meshes 1 and 2, the R_g values are maintained at all separation distances, while in Mesh 2, the GPG decreases as they move away. On the line of the measurement axis, a graph of the touch and step voltage is plotted for insulated grids 1 and 2, for a distance $d=30m$, Figure 24.

3.1.12. Mesh 1 and Mesh 2 are Connected.

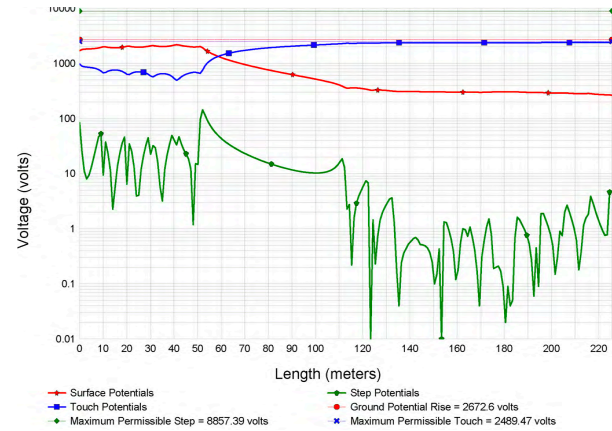
If meshes 1 and 2 are connected, the leak fault currents are the same, and the potentially dangerous voltages are generated due to their geometric symmetry. The meshes may be intentionally or unintentionally attached through various metal installations such as cables, pipes, or metal rails.

Table 11. Voltages touch, step, R_g , GPG.Mesh 1 and 2 joined

| d(m) | Mesh 1 | | | | Mesh 2 | | | |
|------|-----------------|-------|-------------|---------|-----------------|-------|-------------|---------|
| | Maximum Voltage | | $R_g\Omega$ | GPG | Maximum Voltage | | $R_g\Omega$ | GPG |
| | Touch | Step | V | Touch | Step | V | V | |
| 10 | 600.808 | 52.99 | 0.307 | 1731.01 | 600.808 | 54.4 | 0.307 | 1731.01 |
| 20 | 576.057 | 51.15 | 0.296 | 1668.63 | 576.057 | 53.41 | 0.296 | 1668.63 |
| 30 | 557.325 | 49.72 | 0.287 | 1619.07 | 557.325 | 51.84 | 0.287 | 1619.07 |
| 40 | 542.037 | 48.53 | 0.28 | 1577.25 | 542.037 | 50.55 | 0.28 | 1577.25 |
| 50 | 526.901 | 47.48 | 0.273 | 1540.53 | 526.901 | 49.42 | 0.273 | 1540.53 |
| 60 | 517.206 | 46.51 | 0.268 | 1507.44 | 517.206 | 48.38 | 0.268 | 1507.44 |
| 70 | 506.565 | 45.63 | 0.262 | 1477.04 | 506.565 | 47.44 | 0.262 | 1477.04 |
| 80 | 496.696 | 44.79 | 0.257 | 1448.7 | 496.696 | 46.54 | 0.257 | 1448.7 |
| 90 | 487.437 | 43.99 | 0.252 | 1422.2 | 487.437 | 45.7 | 0.252 | 1422.2 |
| 100 | 478.677 | 43.22 | 0.248 | 1397.06 | 478.677 | 44.89 | 0.248 | 1397.06 |
| 110 | 514.775 | 47.22 | 0.263 | 1481.65 | 514.775 | 48.88 | 0.263 | 1481.65 |
| 120 | 462.371 | 41.78 | 0.24 | 1350.29 | 462.371 | 43.37 | 0.24 | 1350.29 |

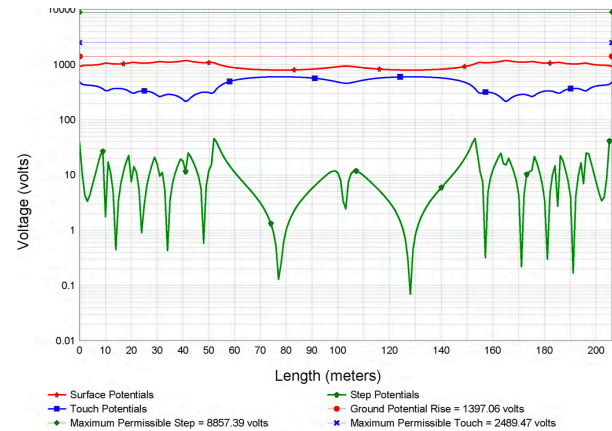
The union of the two meshes is considered using an isolated cable with the same characteristics as those that make up the respective meshes, obtaining similarity between MTV and MSV in both meshes, see table 10. In an electrical failure, the voltage values are reflected in mesh 2. It indicates the need for an exhaustive analysis; before intentionally connecting mesh 1 with mesh 2, it is necessary to check if the security measures applied in the Mesh 2 installations can build up to dangerous voltages and ground currents. On the other hand, the parallel connection of the grounding system meshes decreases the ground currents and the TTV associated with mesh 1. The

TTV and TSV metrics at a distance $d=30m$ are shown in Figure 25.

**Figure 25.** Voltages touch and step - on the measuring axis of mesh 1 and mesh 2 connected

3.1.13. Mesh 1 and Mesh 2 without Connection - Mesh 2 Underground.

Distribution source transformer stations are often located close to surrounding buildings in urban areas. On the other hand, GS's are often intentionally or unintentionally interconnected; therefore, they tend to have a very low R_g . It is essential to assess potentially dangerous voltages that may appear on the ground grid of an adjacent building closest to the substation.

**Figure 26.** Touch and step voltages on the measuring axis - Mesh 1 and Mesh 2 isolated - Mesh 2 grounded**Table 12.** Voltages touch, step, R_g , GPG Mesh 1 - Mesh 2 grounded

| d(m) | Mesh 1 | | | Mesh 2 | | | | |
|------|-----------------|-------|-------|-----------------|---------|-------|-------|---------|
| | Maximum Voltage | | GPG | Maximum Voltage | | GPG | | |
| | Touch | Step | V | Touch | Step | V | | |
| 10 | 989.093 | 98.77 | 0.46 | 2589.35 | 2101.29 | 31.52 | 0.46 | 549.539 |
| 20 | 981.739 | 96.67 | 0.46 | 2638.14 | 2202.31 | 20.62 | 0.46 | 483.27 |
| 30 | 978.94 | 95.97 | 0.474 | 2656 | 2268.01 | 15.1 | 0.474 | 423.433 |
| 40 | 977.658 | 95.68 | 0.474 | 2663.49 | 2320.62 | 12.7 | 0.474 | 367.376 |
| 50 | 976.7981 | 95.47 | 0.474 | 2669.13 | 2355.08 | 10.32 | 0.474 | 333.388 |
| 60 | 976.309 | 95.36 | 0.474 | 2672.6 | 2382.59 | 8.57 | 0.474 | 305.593 |

The potential distribution on the ground surface of grid 1, where the source distribution substation is located, and grid 2, which represents the ground grid of the building closest to the substation, is calculated. The calculations are made assuming that the ground mesh of the building is connected to the ground meshes of the surrounding buildings; it is assumed that the meshes of the structures have the same characteristics and technical parameters equal to mesh 1. The simulation for the two meshes is done by varying their distance, starting from 10 to 60 meters, obtaining $TTV=2489.47$ V and $TSV=8857.39$ V. In the situation in urban areas, the MTV in the neighboring building for $d = 30$ presents high values; however, the stepped voltages in the space between the substation and the adjoining installation are higher voltages for the grids connected. The transfer of dangerous potentials and the technical parameters of the mesh and the ground depend mainly on the value of the fault current. A considerable distance between nearby meshes does not guarantee a decrease in the transfer of dangerous potentials. In electrical substations, the resistivity value of the surface layer is an important parameter to take into account; its value directly influences the TTV and TSV values of the substation and, therefore, the transferred potential gradients.

4. Conclusions

Based on the scenarios presented in this study with variables of resistivity of the surface layer and different configurations, the variation of the GPG has been determined against several strategies. Technical parameters that appear in GS designs have been related and evaluated, observing how these influence the GPG.

This article presents the simulation and analysis of real potential transfer scenarios between electrical substations and metallic structures. Based on them, results have been obtained that reflect the values of dangerous transfer voltages to metallic structures near a substation, exceeding the TTV and TSV allowed in a GS. Measures and procedures taken into account to reduce transfer voltages in the design and construction of GS are indicated.

The values of short-circuit currents, soil resistivity, distances, and location between nearby metal structures, among other design parameters, influence the transfers of electrical potentials between a substation and adjoining metal structures. It is essential to consider the GPG generated in a GS outside the substation area, the interference effects of potentials generated by the existence of metal structures, and the GS close to the substation.

In nearby grids, an analysis is made of the potentially dangerous situations that may appear when transferring the potentials generated by the ground

fault currents to the grids and nearby ground equipment and the personnel protected by them. In designs of cathodic protection systems for pipelines in oil stations, interferences between GS's connected to the substation grid with cathodic protection systems are avoided as much as possible. Otherwise, the problem should be deepened, proposing suitable solutions to this interference, which would prevent compromising the effectiveness of the cathodic protection system.

Detailed scenario analysis is performed when the nearby grid is with other grounded objects; these circumstances are necessary for installing substations in urban areas. The analysis carried out in the document has shown that in case of ground faults in an unintentional connection of ground networks, it can cause high TTV and TSV in nearby meshes, which can lead to severe risks for the human being who transmits them.

References

- [1] J. Nahman and D. Salamon, "Mutual interference of neighboring grounding systems and approximate formulation," *Electric Power Systems Research*, vol. 151, pp. 166–173, 2017. [Online]. Available: <https://doi.org/10.1016/j.epsr.2017.05.029>
- [2] L. Fu, "The influence of Urban Substation on Neighbouring Metal Grounding System," *Journal of Physics: Conference Series*, vol. 1176, no. 4, 2019. [Online]. Available: <https://doi.org/10.1088/1742-6596/1176/4/042051>
- [3] L. Neamt, H. Balan, O. Chiver, and A. Hotea, "Considerations about Substation Grounding System Design," in *Proceedings of 2019 8th International Conference on Modern Power Systems, MPS 2019*. Institute of Electrical and Electronics Engineers Inc., 2019. [Online]. Available: <https://doi.org/10.1109/MPS.2019.8759737>
- [4] M. L. Di Silvestre, L. Dusonchet, S. Favuzza, S. Mangione, L. Mineo, M. Mitolo, E. R. Sanseverino, and G. Zizzo, "On the Interconnections of HV-MV Stations to Global Grounding Systems," *IEEE Transactions on Industry Applications*, vol. 55, no. 2, pp. 1126–1134, 2019. [Online]. Available: <https://doi.org/10.1109/TIA.2018.2875383>
- [5] G. Aiello, S. A. Rizzo, S. Alfonzetti, and N. Salerno, "Computation of Transferred Potentials from Grounding Grids by Means of Hybrid Methods," in *Proceedings - 2018 IEEE International Conference on Environment and Electrical Engineering and 2018 IEEE Industrial and Commercial Power Systems Europe, IEEEIC/I and CPS Europe 2018*. Institute of Electrical and Electronics Engineers Inc., 2018. [Online]. Available: <https://doi.org/10.1109/IEEEIC.2018.8493916>

- [6] L. Popović, “Preliminary testing and assessment of safety conditions of HV substations located in urban areas,” *Electric Power Systems Research*, vol. 195, 2021. [Online]. Available: <https://doi.org/10.1016/j.epsr.2021.107111>
- [7] C. Martineac and R. N. Hasanah, “Influence of soil resistivity on substations earth grounding system,” in *Proceedings of 2019 8th International Conference on Modern Power Systems, MPS 2019*. Institute of Electrical and Electronics Engineers Inc., 2019. [Online]. Available: <https://doi.org/10.1109/MPS.2019.8759796>
- [8] G. Cafaro, P. Colella, P. Montegiglio, E. Pons, R. Tommasini, F. Torelli, and G. Valtorta, “Ground Resistance of Buried Metallic Parts in Urban Areas: An Extensive Measurement Campaign,” *IEEE Transactions on Industry Applications*, vol. 53, no. 6, pp. 5209–5216, 2017. [Online]. Available: <https://doi.org/10.1109/TIA.2017.2748502>
- [9] W. A. Byrd, “Below Grade Coated Direct Imbedded Steel Pole Corrosion Failures With Solutions,” *IEEE Power and Energy Technology Systems Journal*, vol. 6, no. 1, pp. 41–46, 2018. [Online]. Available: <https://doi.org/10.1109/JPETS.2018.2884974>
- [10] Q. Lv, Z. Xiang, X. Li, J. Ai, S. Liu, and C. Zhang, “Research on overvoltage protection strategy of oil-gas pipeline based on non-metallic grounding material,” in *2019 4th International Conference on Intelligent Green Building and Smart Grid, IGBSG 2019*. Institute of Electrical and Electronics Engineers Inc., 2019, pp. 97–102. [Online]. Available: <https://doi.org/10.1109/IGBSG.2019.8886338>
- [11] S. A. H. Mohammed and I. M. Abdulbaqi, “Numerical Study and Design of an Impressed Current Cathodic Protection System for Buried Metallic Pipes,” in *2018 3rd Scientific Conference of Electrical Engineering, SCEE 2018*. Institute of Electrical and Electronics Engineers Inc., 2018, pp. 95–100. [Online]. Available: <https://doi.org/10.1109/SCEE.2018.8684076>
- [12] E. Inga and R. Hincapié, “Creación de artículos académicos basados en minería de datos y Web 2.0 para incrementar la producción científica en ingeniería,” *Revista Educación en Ingeniería*, vol. 10, no. 20, pp. 65–74, 2015. [Online]. Available: <https://bit.ly/3MX1Woz>
- [13] T. H. Shabangu, P. Shrivastava, B. T. Abe, K. B. Adedeji, and P. A. Olubambi, “Influence of AC interference on the cathodic protection potentials of pipelines: Towards a comprehensive picture,” in *2017 IEEE AFRICON: Science, Technology and Innovation for Africa, AFRICON 2017*. Institute of Electrical and Electronics Engineers Inc., 2017, pp. 597–602. [Online]. Available: <https://doi.org/10.1109/AFRCON.2017.8095549>
- [14] G. Liu, G. Jiang, Z. Zhang, D. Mei, and Y. Zheng, “Research on the influence of DC current overflowing on grounding electrode corrosion,” in *Proceedings of 2017 IEEE 3rd Information Technology and Mechatronics Engineering Conference, ITOEC 2017*, vol. 2017-Janua. Institute of Electrical and Electronics Engineers Inc., 2017, pp. 291–295. [Online]. Available: <https://doi.org/10.1109/ITOEC.2017.8122438>
- [15] M. G. Mahlobo, P. Mjwana, M. N. Tladi, B. A. Obadele, P. A. Olubambi, and P. Refait, “Evaluation of cathodic protection performance of carbon steel pipeline buried in soil: A review,” in *2018 IEEE 9th International Conference on Mechanical and Intelligent Manufacturing Technologies, ICMIMT 2018*, vol. 2018-Janua. Institute of Electrical and Electronics Engineers Inc., 2018, pp. 37–43. [Online]. Available: <https://doi.org/10.1109/ICMIMT.2018.8340417>
- [16] B. Zhang, F. Cao, X. Meng, Y. Liao, and R. Li, “Numerical approach of impressed potential on buried pipelines near high-voltage DC grounding electrodes,” *IET Generation, Transmission and Distribution*, vol. 12, no. 5, pp. 1177–1182, 2018. [Online]. Available: <https://doi.org/10.1049/iet-gtd.2017.1436>
- [17] F. Babaghayou, B. Zegnini, and T. Seghier, “Experimental model investigation of the corrosion of buried steel pipelines with cathodic protection near high voltage power lines,” *Proceedings of 2016 International Conference on Electrical Sciences and Technologies in Maghreb, CISTEM 2016*, pp. 1–6, 2017. [Online]. Available: <https://doi.org/10.1109/CISTEM.2016.8066812>
- [18] H. Xuedong, Y. Wei, L. Xinghua, S. Xiangping, and H. Xuyin, “Analysis of grounding status of substation secondary system and improvement measures,” in *China International Conference on Electricity Distribution, CICED, 2018*, pp. 1479–1483. [Online]. Available: <https://doi.org/10.1109/CICED.2018.8592194>
- [19] M. Di Silvestre, L. Dusonchet, S. Favuzza, S. Mangione, L. Mineo, M. Mitolo, E. Sanseverino, and G. Zizzo, “Interconnections criteria of grounding grids in global grounding systems,” in *Conference Record - Industrial and Commercial Power Systems Technical Conference*, vol.

- 2018-May, 2018, pp. 1–8. [Online]. Available: <https://doi.org/10.1109/ICPS.2018.8369974>
- [20] R. Pereira Sodre, B. Lopes Pereira, L. Leite Sidrim, J. F. Almeida, and C. L. S. Souza Sobrinho, “Optimization of Grounding Grids Design for a Square-Shaped Mesh,” *IEEE Latin America Transactions*, vol. 16, no. 1, pp. 135–139, 2018. [Online]. Available: <https://doi.org/10.1109/TLA.2018.8291465>
- [21] C. Payshetti, H. Jadhav, and S. Kulkarani, “Analysis of grounding grid of substation,” in *Proceedings of IEEE International Conference on Circuit, Power and Computing Technologies, ICCPCT 2017*, 2017. [Online]. Available: <https://doi.org/10.1109/ICCPCT.2017.8074259>
- [22] I. Kasim, S. Abduh, and N. Fitryah, “Grounding system design optimization on 275 KV betung substation based on IEEE standard 80-2000,” in *QiR 2017 - 2017 15th International Conference on Quality in Research (QiR): International Symposium on Electrical and Computer Engineering*, vol. 2017-Decem. Institute of Electrical and Electronics Engineers Inc., 2017, pp. 400–407. [Online]. Available: <https://doi.org/10.1109/QIR.2017.8168519>
- [23] M. D. Kavimandan and A. M. Silva, “Impacts of Existing Infrastructure on Soil Resistivity,” *Proceedings of the IEEE Power Engineering Society Transmission and Distribution Conference*, vol. 2020-October, pp. 20–23, 2020. [Online]. Available: <https://doi.org/10.1109/TD39804.2020.9299899>
- [24] A. Raizer, W. Valente, and V. L. Coelho, “Development of a new methodology for measurements of earth resistance, touch and step voltages within urban substations,” *Electric Power Systems Research*, vol. 153, pp. 111–118, 2017. [Online]. Available: <https://doi.org/10.1016/j.epsr.2017.01.025>
- [25] M. Abdaldaim, P. Wang, and L. Li, “The design of 110kV substation grounding grid with high resistivity soil,” in *2017 IEEE 6th Asia-Pacific Conference on Antennas and Propagation, APCAP 2017-Proceeding*. Institute of Electrical and Electronics Engineers Inc., 2018, pp. 1–3. [Online]. Available: <https://doi.org/10.1109/APCAP.2017.8420847>
- [26] X. Wu, V. Simha, R. J. Wellman, M. Thakur, and S. S. Dimpfl, “Substation Grounding Study Input Parameter Sensitivity Analysis and Simulation Strategies,” in *IEEE Transactions on Industry Applications*, vol. 55, no. 3. Institute of Electrical and Electronics Engineers Inc., 2019, pp. 2272–2280. [Online]. Available: <https://doi.org/10.1109/TIA.2018.2885475>
- [27] D. S. Gazzana, A. B. Tronchoni, R. C. Leborgne, M. Telló, and A. S. Bretas, “Numerical Technique to the Evaluation of Multiple Grounding Electrodes Coupled by the Soil in High Voltage Substations,” in *Proceedings - 2019 IEEE International Conference on Environment and Electrical Engineering and 2019 IEEE Industrial and Commercial Power Systems Europe, EEEIC/I and CPS Europe 2019*. Institute of Electrical and Electronics Engineers Inc., 2019. [Online]. Available: <https://doi.org/10.1109/EEEIC.2019.8783554>
- [28] C. Gomes and M. Izadi, “Electrical Isolation of Two Earthing Systems under Lightning Conditions with TiO₂ Nano Fluid Barrier,” *2019 15th International Symposium on Lightning Protection, SIPDA 2019*, no. October, pp. 1–5, 2019. [Online]. Available: <https://doi.org/10.1109/SIPDA47030.2019.8951640>
- [29] P. R. Bonda and M. K. Mishra, “Optimized Design of Earthing System for Substations with High Soil Resistivity and Limited Plot Area,” in *2018 20th National Power Systems Conference, NPSC 2018*. Institute of Electrical and Electronics Engineers Inc., 2018. [Online]. Available: <https://doi.org/10.1109/NPSC.2018.8771780>
- [30] M. Salam, Q. Rahman, S. Ang, and F. Wen, “Soil resistivity and ground resistance for dry and wet soil,” *Journal of Modern Power Systems and Clean Energy*, vol. 5, no. 2, pp. 290–297, 2017. [Online]. Available: <https://doi.org/10.1007/s40565-015-0153-8>
- [31] C. Cardoso, L. Rocha, A. Leiria, and P. Teixeira, “Validation of an integrated methodology for design of grounding systems through field measurements,” in *CIREd - Open Access Proceedings Journal*, vol. 2017, no. 1, 2017, pp. 897–901. [Online]. Available: <https://doi.org/10.1049/oap-cired.2017.0452>
- [32] K. P. Sengar and K. Chandrasekaran, “Designing of cost minimum substation grounding grid system using DE, SCA, and HDESCA techniques,” *IET SCIENCE MEASUREMENT & TECHNOLOGY*, vol. 13, no. 9, pp. 1260–1267, 2019. [Online]. Available: <https://doi.org/10.1049/iet-smt.2019.0021>
- [33] M. Campaña, P. Masache, E. Inga, and D. Carrión, “Estabilidad de tensión y compensación electrónica en sistemas eléctricos de potencia usando herramientas de simulación,” *Ingenius*, vol. 2, no. 1, 2022. [Online]. Available: <https://doi.org/10.17163/ings.n28.2022.07>
- [34] M. H. Elmashtoly, H. I. Anis, and A. Emam, “Mitigating Hazardous Potentials Near Pipelines Using

- Passive Grounding Grids,” *IEEE Access*, vol. 9, pp. 121 957–121 963, 2021. [Online]. Available: <https://doi.org/10.1109/ACCESS.2021.3109309>
- [35] L. Amaya and E. Inga, “Location of Harmonic Distortions in Electrical Systems using Compressed Sensing,” *Ingeniería y Competitividad*, vol. 24, no. 1, p. 15, 2022. [Online]. Available: <https://bit.ly/3xA4zqI>
- [36] N. Permal, M. Osman, A. M. Ariffin, and M. Z. Abidin Ab Kadir, “Effect of non-homogeneous soil characteristics on substation grounding-grid performances: A review,” *Applied Sciences (Switzerland)*, vol. 11, no. 16, 2021. [Online]. Available: <https://doi.org/10.3390/app11167468>
- [37] P. Musil, P. Mlynek, J. Slacik, and J. Pokorny, “Simulation-based evaluation of the performance of broadband over power lines with multiple repeaters in linear topology of distribution substations,” *Applied Sciences (Switzerland)*, vol. 10, no. 19, pp. 1–24, 2020. [Online]. Available: <https://doi.org/10.3390/app10196879>
- [38] B. Anggoro, R. S. Utami, and L. Handayani, “Optimal Design of Grounding System Substation, Case Study : 275/150 kV Sigli Substation,” *Proceedings of the 2nd International Conference on High Voltage Engineering and Power Systems: Towards Sustainable and Reliable Power Delivery, ICHVEPS 2019*, vol. 1, 2019. [Online]. Available: <https://doi.org/10.1109/ICHVEPS47643.2019.9011064>
- [39] X. Tian, Z. Lan, F. Huo, Z. Huang, S. Huang, Y. Ding, J. Geng, X. Yan, and Y. Liu, “Calculation of electric field on substation equipment considering AC Ion flow field,” *Mathematical Problems in Engineering*, vol. 2020, 2020. [Online]. Available: <https://doi.org/10.1155/2020/3914872>
- [40] Z. G. Datsios and P. N. Mikropoulos, “Safety performance evaluation of typical grounding configurations of MV/LV distribution substations,” *Electric Power Systems Research*, vol. 150, pp. 36–44, 2017. [Online]. Available: <https://doi.org/10.1016/j.epsr.2017.04.016>
- [41] Z. Liu, W. Shi, and B. Zhang, “Numerical analysis of transient performance of grounding grid with lightning rod installed on multi-grounded frame,” *Energies*, vol. 14, no. 12, pp. 1–13, 2021. [Online]. Available: <https://doi.org/10.3390/en14123392>
- [42] V. P. Androvitsaneas, K. D. Damianaki, C. A. Christodoulou, and I. F. Gonos, “Effect of soil resistivity measurement on the safe design of grounding systems,” *Energies*, vol. 13, no. 12, 2020. [Online]. Available: <https://doi.org/10.3390/en13123170>
- [43] B. KÜchler, U. Schmidt, and J. Hänsch, “Harmonic current distribution in grounding systems of cabled medium voltage grids during single-pole ground fault,” *Energies*, vol. 14, no. 4, 2021. [Online]. Available: <https://doi.org/10.3390/en14041110>
- [44] F. Sinchi-sinchi, C. Coronel-naranjo, A. Barragán-escandón, and F. Quizhpi-palomeque, “Soil Treatment to Reduce Grounding Resistance by Applying Low-Resistivity Material (LRM) Implemented in Different Grounding Systems Configurations and in Soils with Different Resistivities,” *Applied Sciences*, vol. 12, 2022. [Online]. Available: <https://doi.org/10.3390/app12094788>
- [45] F. Holik, L. H. Flå, M. G. Jaatun, S. Y. Yayilgan, and J. Foros, “Threat Modeling of a Smart Grid Secondary Substation,” *Electronics (Switzerland)*, vol. 11, no. 6, pp. 1–21, 2022. [Online]. Available: <https://doi.org/10.3390/electronics11060850>